

Effect of Copper as an Alloying Element on Microstructure and Mechanical Properties of Grey Cast Iron

Himanshu Shekhar Mishra¹  · Rina Sahu¹ ·
D. S. Padan²

Received: 3 August 2022 / Accepted: 2 February 2023 / Published online: 3 March 2023
© The Indian Institute of Metals - IIM 2023

Abstract In the present work, the effect of copper (0.25–1 wt.%) on the microstructural and mechanical properties of the grey cast iron has been examined keeping the Sn constant. The results showed that the pearlite formation in the cast microstructure increases as the copper content increases. The graphite flake length, area, and aspect ratio decrease while the edge roundness increases with the copper addition. With the addition of copper, the mechanical properties such as tensile strength and yield strength increase drastically, while impact strength decreases. The optimum Cu content for good mechanical and microstructural properties is found to be 0.48 wt.%.

Keywords Copper alloying · Grey cast iron · Pearlite microstructure · Graphite flakes

1 Introduction

Grey cast iron holds 50% of the total share in the overall metal castings production, of which 32% is used for automobile castings. Usually, copper and tin are extensively used as alloying elements in automobile applications to favor the pearlitic microstructure and avoid graphite degeneracy, carbide defects, and enhance the mechanical properties [1–3]. Tsujikawa et al. [4] studied the effect of copper (0.1–0.69 wt.%) on the microstructural and mechanical properties of spheroidal grey cast iron. They found that the

pearlite fraction in the cast iron increases abruptly when the copper content exceeds 0.4 wt.%, and it provides strengthening and hardening of cast iron. They also noted that there is no excess copper-rich phase observed in the microstructures at all compositions. Copper also improves corrosion resistance, antifriction, wear properties, and reduces the chilling tendency in grey cast iron [5]. Tin is an excellent pearlite promoter and it also acts as a diffusion barrier for carbon transfer between austenite and ferrite, and its value is normally kept in the range of 0.04–0.1 wt.%. Addition of Sn over 0.1 wt.% causes embrittlement and soundness in cast iron [6, 7].

As discussed, graphite morphology has an adverse effect on the mechanical properties of cast iron. There are two major graphite morphologies in grey cast iron, (i) flake type and (ii) spheroidal. Spheroidal graphite cast irons have improved ductility and fracture toughness [4, 8], while the flake type has good lubrication properties, damping capacities, thermal conductivity, and compressive strength [9]. The cylinder blocks and heads used in vehicle engines require good lubrication and damping properties along with adequate mechanical properties as well as they need to be cost-effective. Usually, alloying elements like Mo, Mn, Ni, Sn, and Cu metals are added in flake-type grey cast irons to obtain the required microstructure or mechanical properties [5]. Among all, copper is widely available and the cheapest in the market which aids in minimizing the overall cost of manufacturing. Hence, the major aim of this paper is to study the effect of the cheaper alloying element copper on the microstructural and mechanical properties of the grey cast irons (in presence of tin) used in cylindrical blocks and heads.

✉ Himanshu Shekhar Mishra
hsmishra005@gmail.com

¹ Department of Metallurgical and Materials Engineering,
NIT-Jamshedpur, Jamshedpur, Jharkhand 831014, India

² Foundry Division, Tata Motors Limited, Jamshedpur,
Jharkhand 831010, India

2 Experimental Procedure

2.1 Materials Used

Foundry scrap (20%), generated inside the Tata Motors Jamshedpur plant, and steel scrap (80%) were used as the source of iron in the present study. Petroleum coke from the Barauni refinery, Bihar (India), was used as the source of carbon alloying during melting. Ferrosilicon lumps and fines collected from Kalinga Alloys Private Limited, Bhubaneswar, Orissa (India), were used as the silicon source. Pure Cu and Sn (99.5 wt.%) supplied by the Metals and Minerals Trading Corporation of India Limited was used as pearlite stabilizers. The composition and size analysis of the charge materials are given in Table 1.

2.2 Sample Preparation and Characterization

The master metal for the grey cast iron was prepared in a medium frequency induction furnace with a capacity of 5 MT and a power rating of 3800 kW/120 Hz. Petroleum coke, and the mixer of steel scrap (80%) and foundry returns (20%) were charged layer wise in the induction furnace for melting. The total mass of the melt was 5 MT. After the complete melting of the master alloy, the lumps of ferrosilicon were added into the furnace to fix the silicon content in the master metal. To ensure the homogeneity of the melt, it was kept at 1500 °C for 5–10 min. The slag formed on the melt surface was skimmed off and then the melt was poured into a preheated ladle (at 900–1000 °C, 1 MT capacity) for alloying with copper and tin. The temperature of the melt was maintained at 1470–1480 °C at the time of alloying. The effect of copper (0.11 wt.%, 0.22 wt.%, 0.48 wt.%, 0.72 wt.%, and 0.9 wt.%) and tin (~0.05 wt.%) alloy content was studied. A pellet sample was collected and sent for spectroscopic analysis in each step to examine the melt composition.

The influence of copper and tin on the microstructural and mechanical properties of the grey cast iron was analyzed by the microstructural variations in the chill proportion

of the wedge sample, tensile test, Charpy test, and hardness test. The sample preparation for the different analyses used in the present study is given in Fig. 1. The alloy melt obtained from the ladle was poured into a resin bonded sand cylindrical mold (dimensions: 230 × 100 × 100 mm with a draft of 1 degree to 230 × 90 × 90 mm with a round hole of the diameter of 38 mm) (See Fig. 1a). The ferrosilicon powder was added into the cylindrical mold before pouring the melt so as to minimize the chill proportion on the edges due to rapid cooling. Fe–Si alloy powder (0.2 wt.%) was added to the mold to minimize the chill portion. These cylindrical ingots were directly used for making tensile test specimens, hardness testing, and Charpy test samples and calibrated the respective mechanical properties according to the ASTM standards ASTM E 8, ASTM E10 [10], and ASTM D256-93 [7], respectively. Wedge samples were prepared by pouring the melt in a resin-coated sand pattern, as shown in Fig. 1h, to determine the chill proportions according to the ASTM A367-60 standards [11]. Coins were prepared using a copper mold, as shown in Fig. 1g. After the solidification, the samples were air-cooled to obtain the final test specimen for the microstructural examination. Each mechanical testing procedure was repeated thrice and the average was taken for calibration. Leica steel expert Version 2.0 software was used for the length, width, area, roundness, and aspect ratio measurements of flakes formed in the grey cast iron under different conditions.

2.3 Characterization

The X-ray fluorescence technique was used to examine the composition of the master and the alloyed samples, which are given in Table 2. The microstructure of the master metal, alloyed metal, and fracture surfaces of the samples were examined by using optical and scanning electron microscopy. Optical microscope Leica DM 2500 (Germany), supported with image analyzing software (LAS V4.8) for qualitative and quantitative measurements of microstructural features, was used to find out the graphite flake proportion

Table 1 Composition of the raw materials used

Materials	Compositions						Size/weight/forms	Purity
	%C	%Si	%Mn	%Cr	%S	%P		
Steel Scrap	0.1	0.1	0.50	0.40	<0.06	<0.06	8 × 4 × 4 inches	Clean, non-oily, non-rusty,
Foundry returns	3.35	1.8	0.55	0.50	0.05	0.05	8 × 4 × 4 inches	No wet, Sand and dust free
Petroleum coke	80.0	–	–	–	–	–	Granular form	–
Ferro-silicon	–	70.0	–	–	–	–	Lump form (1–2 kg)	–
Ferro-silicon powder for inoculation	–	70.0	–	–	–	–	– 18 + 50 mesh size (0.2%)	–
Copper	–	–	–	–	–	–	Turnings	100%
Tin	–	–	–	–	–	–	Lump form	99.5%

Fig. 1 The samples were collected for the mechanical testing and micrographic examination of the grey cast alloys, **a** Cylindrical resin coated sand mold for the tensile and Charpy test samples preparation, **b** Solidified ingot obtained from the cylindrical mold, **c** The tensile test specimen, **d** The Charpy test specimen, **e** Resin-coated sand mold for wedge casting preparation, **f** Solidified wedge casting sample, and **g** Broken wedge casting showing chill (white region) portion

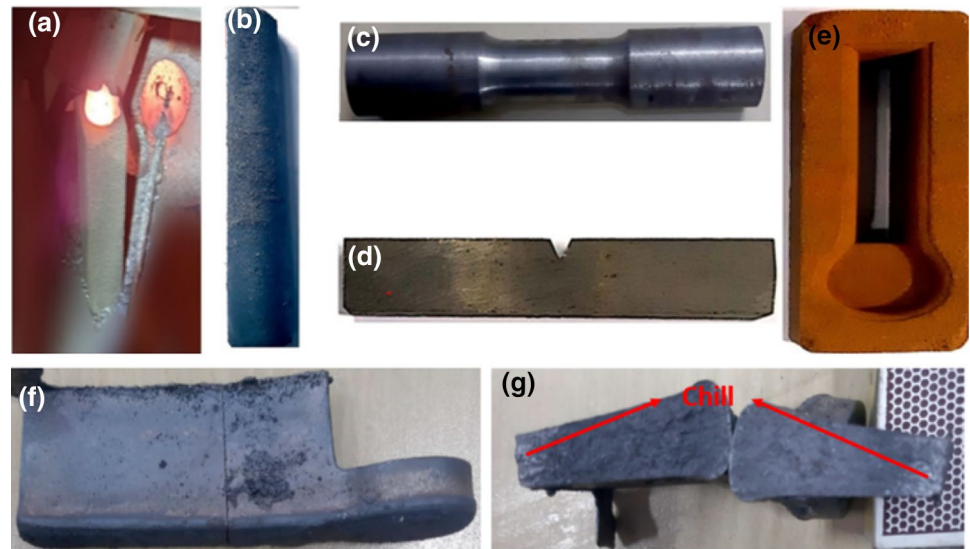


Table 2 Composition of the base metal and alloys

Sample Code	%C	%Mn	%Si	%S	%P	%Cr	%Cu	%Sn	%Mo	%Ni	%V	%Al	%Ti	%Pb	%B	%Fe
C0	3.38	0.75	1.89	0.053	0.039	0.091	0.11	0.010	0.005	0.026	0.004	0.003	0.006	0.001	0.001	93.63
C1	3.35	0.74	1.85	0.056	0.038	0.089	0.22	0.051	0.003	0.026	0.004	0.003	0.006	0.001	0.001	93.56
C2	3.34	0.73	1.84	0.054	0.035	0.087	0.48	0.052	0.005	0.025	0.005	0.002	0.005	0.001	0.001	93.38
C3	3.31	0.75	1.82	0.058	0.036	0.086	0.72	0.048	0.004	0.021	0.006	0.003	0.005	0.002	0.002	93.13
C4	3.33	0.74	1.87	0.054	0.038	0.085	0.90	0.052	0.005	0.026	0.006	0.004	0.006	0.003	0.003	92.92

and size distribution. The samples were analyzed in un-etched conditions. The ferrite, pearlite, and cementite phases present in the samples were studied by etching the polished samples with 4 wt.% nital solution. SEM (SIGMA Carl Zeiss Germany) equipped with energy dispersive X-ray spectroscopy (EDX Model Octane Plus, AMETEK, USA) was used for the microstructural and fracture surface analyses. The X-ray diffraction patterns of the grey cast iron samples were obtained using the Philips X-ray diffractometer with Cu-K α radiation with a wavelength of 1.55 Å.

3 Results and Discussion

3.1 XRD Analysis

The XRD analysis of the grey cast iron alloy samples, with different copper additions, is shown in Fig. 2. It shows that the α -Fe (ferrite) and cementite phases are the major phases identified in all five alloys. The presence of the ferrite phase present in the grey cast iron indicates the pearlite phase in the alloys. The intensity of ferrite phase peaks decreases with an increase in copper content up to 0.75 wt.% and then increases. As copper act as a pearlite stabilizer, it decreases

the free ferrite content in the grey cast iron and this is the reason for the decrease in ferrite peak intensity. Copper addition retards the diffusion of carbon in austenite to promote the pearlite phase formation in presence of co-alloying elements like Mn, Sn, etc. Copper forms solid solutions with γ -iron and α -iron, and the solubility limit is dependent upon the carbon content, temperature, and co-alloying elements. The excess addition of copper (above the solubility limit) segregates on the eutectic structure and shows a negative impact on the conversion of ferrite to pearlite phase; this may be the reason for the increase in free ferrite phase peaks after 0.72% Cu addition [5].

3.2 Microstructure Analysis

The optical microstructures of the master metal and alloyed (Cu, Sn) samples in both etched and un-etched conditions are shown in Fig. 3. The un-etched samples of the master alloy show long and sharp edge graphite flakes in the microstructure. The length-to-width ratio of the graphite flakes decreases with the increase in the copper addition in the grey cast iron from C0 to C4. In the etched samples, the dark region and the white region are pearlite and ferrite, respectively. The effect of copper addition on the percentage

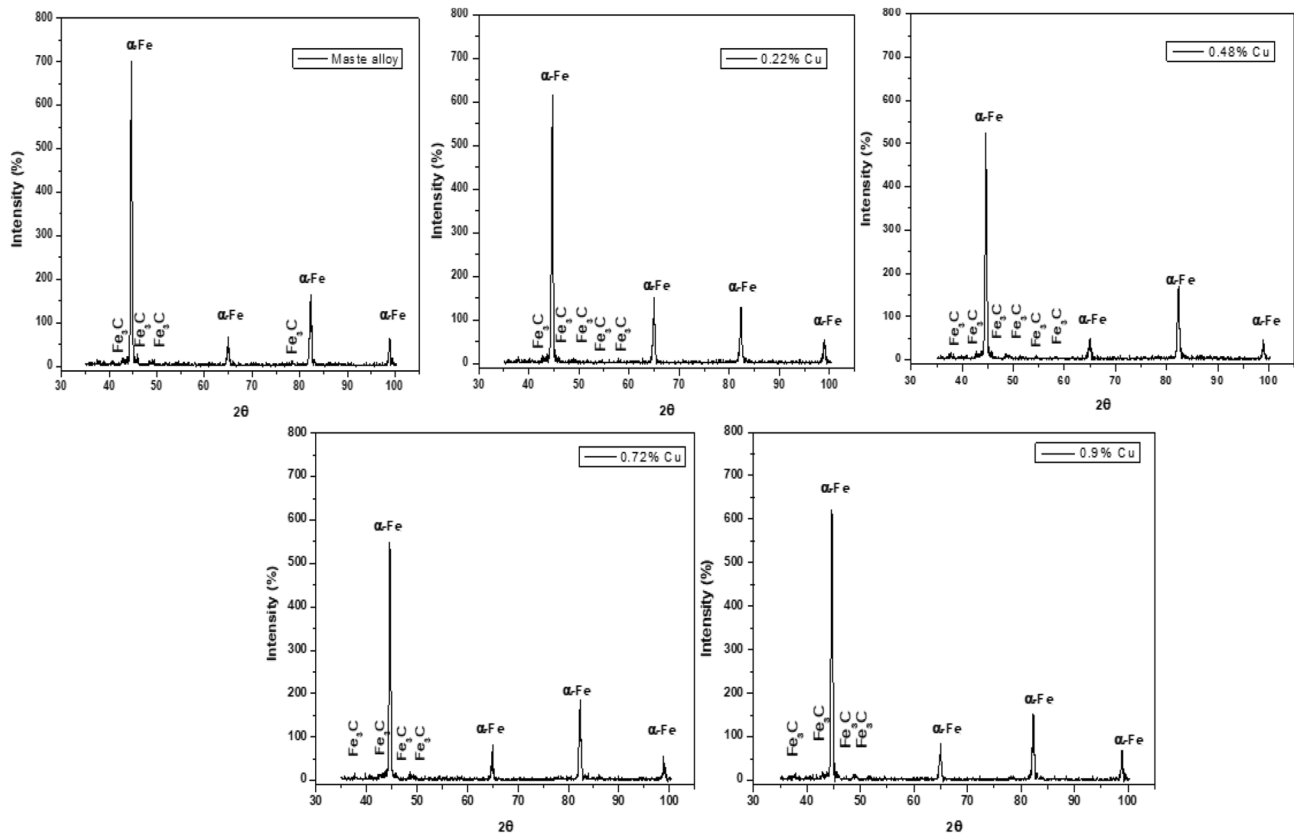


Fig. 2 XRD analysis of the alloys

of graphite flake types, pearlitic and ferritic proportions, and chill depth is calculated from the microstructures using the image software, according to the ASTM standard ASTM A247 [12]. The results are shown in Table 3. From the table, it is evident that the type A graphite flakes with random distribution and uniform sizes are the dominant graphite that forms in the microstructure of all the five alloys (C0, C1, C2, C3, C4). The amount of type A flakes increases with the increase in copper content from C0 to C4. The reason for this is the decrease in the undercooling of the grey cast iron with copper addition, which results in the uniform nucleation of flakes [13–15]. Table 4 shows the variation in the graphite flake length, width, area, aspect-ratio and roundness in C0 to C4 alloys with copper addition. It shows that the aspect ratio decreases while the roundness of the edge increases with an increase in copper content from C0 to C4. The type of graphite flakes and aspect ratio are indications of the extent of changes in graphite morphology in grey cast iron and plays a crucial role in determining the mechanical properties. Generally, type A flakes with a low aspect ratio are preferable for obtaining good mechanical properties in grey cast irons [16, 17]. Chill depth in the casting decreases initially from master alloy (C0) to C1, then further increase in copper content does not show any observable change

in chill depth. Rooney et al. [20] also observed that there was no change in the chill depth with the copper additions beyond 0.9 wt. %.

The cell count micrographs and quantitative analysis variation of the grey cast iron with copper content variation are shown in Fig. 4. It shows that the cell count increases at a rapid rate initially with the increase in copper content from 0.11 to 0.48 wt. %, and then decreases with a further increase in copper content to 0.72 wt. % and 0.90 wt. %. Copper addition to the grey cast iron decreases the eutectic temperatures of cast iron which leads to a decrease in the release of carbon from the melt. This results in extensive pearlitic phase formation during the transformation. The flake formation is aided only by the free carbon that remains after this transition. It is already a proven fact that copper addition increases the mechanical properties by matrix substitution and it does not promote any chilling effect [17–19].

3.3 Mechanical Properties

Figure 5 and Table 5 show the effect of Cu and Sn combined alloying on the mechanical properties of the grey cast iron. Figure 6a shows the variation in tensile strength of the studied grey cast iron with respect to different

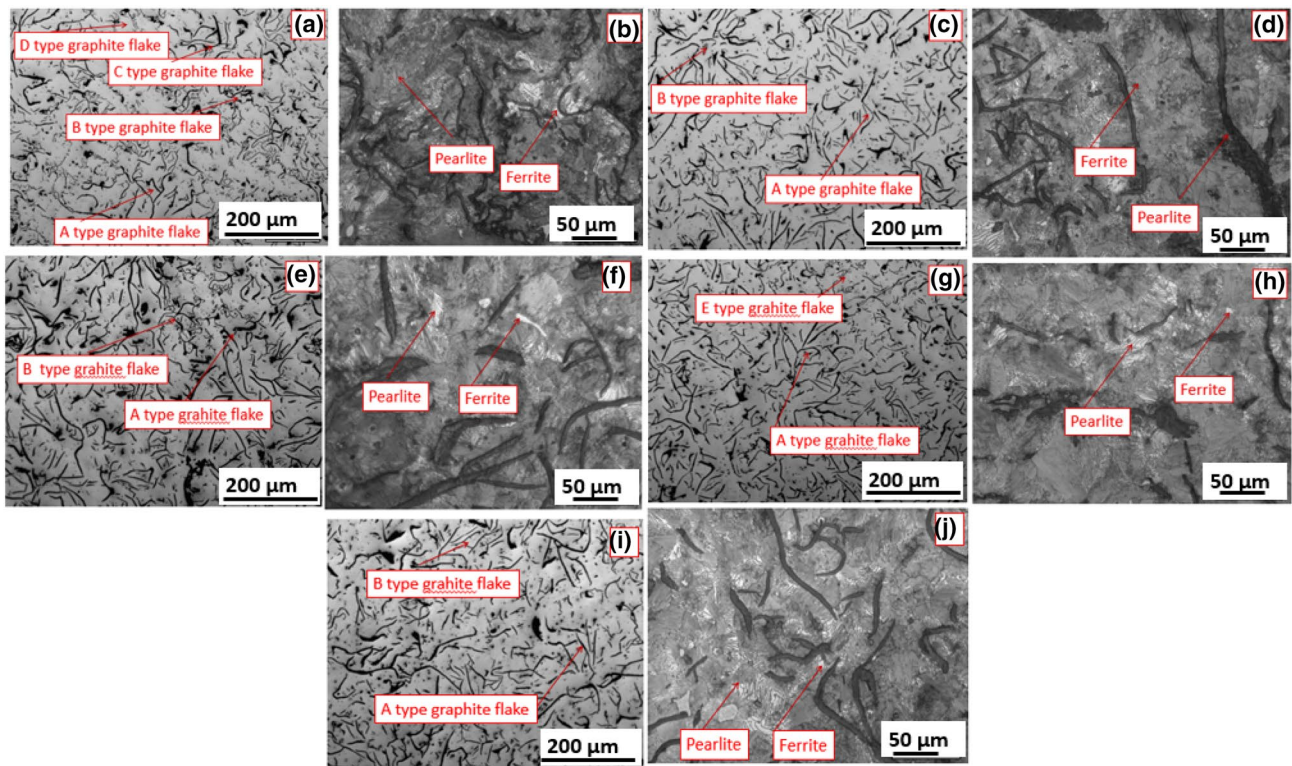


Fig. 3 Optical images of the C0 (a-un-etched, b-etched), C1 (c-un-etched, d-etched), C2 (e-un-etched, f-etched), C3 (g-un-etched, h-etched), and C4 (i-un-etched, j-etched)

Table 3 Chill depth, % Pearlite, % Ferrite and % Flake graphite types A, B, C, D and E

Sample no	Chill depth (mm)	Pearlite (%)	Ferrite (%)	%A type graphite flakes	%B type graphite flakes	%C type graphite flakes	%D type graphite flakes	%E type graphite flakes
C0	6.0	98.56	1.44	95	0.47	1.03	0.24	0.14
C1	5.0	99.30	0.70	98	0.11	0.24	0.11	0.13
C2	5.0	99.58	0.42	99.38	0.19	0.3	0.13	0.00
C3	4.9	99.64	0.85	99.56	0.12	0.26	0.01	0.05
C4	4.9	97.37	2.63	99.59	0.11	0.25	0.00	0.05

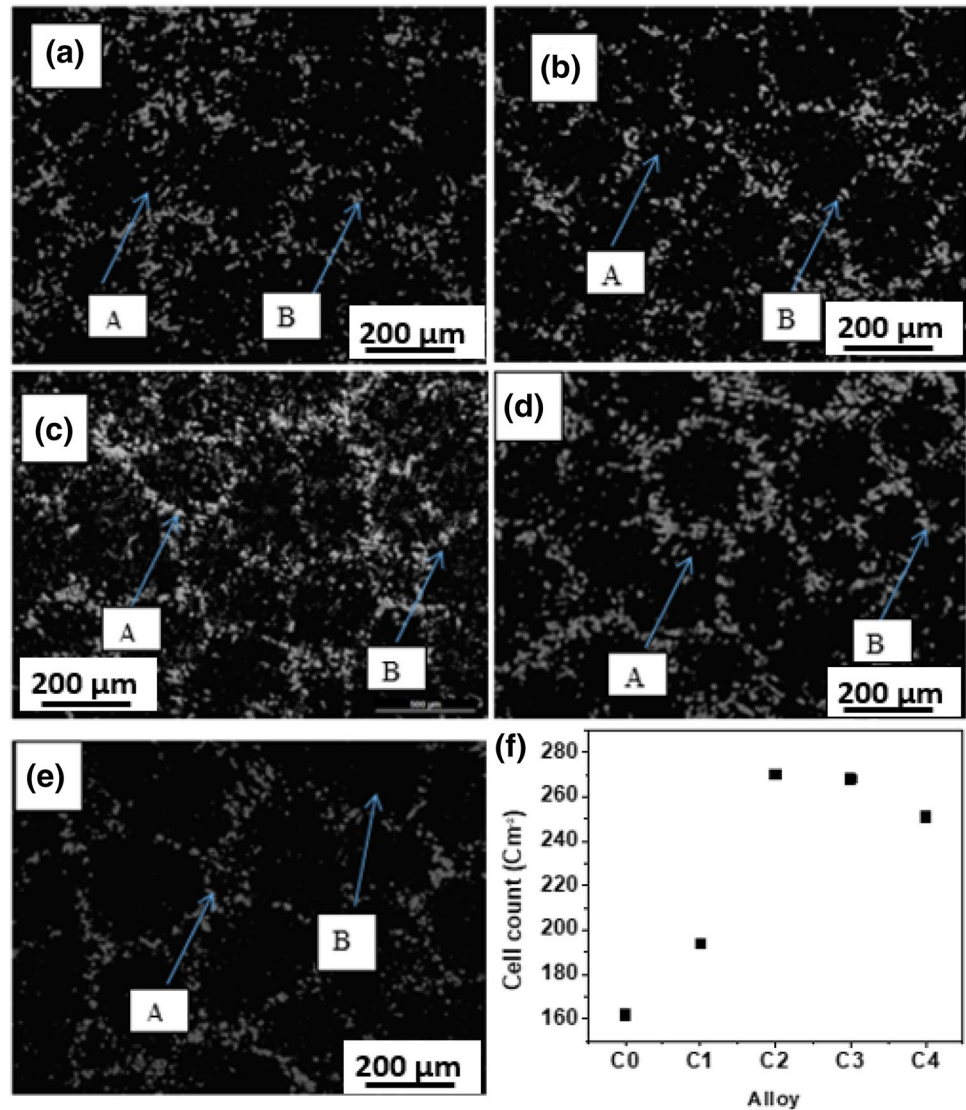
Table 4 Graphite flake length, width, area, aspect ratio and roundness measurement

Sample no	Length (μm)	Width (μm)	Area (μm Sq.)	Aspect ratio	Roundness
C0	312.62	167.65	5071.44	2.47	0.02
C1	296.02	205.93	7279.24	1.71	0.05
C2	295.00	164.41	6962.17	1.83	0.05
C3	238.78	157.83	2107.77	1.65	0.05
C4	217.78	203.22	4826.29	1.51	0.06

alloying conditions. It shows that the tensile strength increases continuously within the order of the alloy C0 < C1 < C2 < C3 and then it get into the C4 alloy. This shows that the tensile strength in grey cast iron increases

with copper addition until 0.72 wt.% and a further increase in copper does not show much difference in tensile strength. The maximum tensile strength of ~310 MPa is obtained in C3 alloy which is composed of 0.72 wt.% Cu.

Fig. 4 Cell count analysis **a** C0 **b** C1 **c** C2 **d** C3 **e** C4 and **f** cell count of the alloys



The reason for the increase in tensile strength from C0 to C3 is due to the increase in the pearlitic to ferrite ratio and cell count within the respective microstructure of the alloys C0, C1, C2, and C3. The increase in the roundness of the graphite flakes from C0 to C3 is also the reason for the increase in tensile strength, which in turn decreases the stress concentration in the alloy upon loading. Similar observations are obtained with the hardness testing of the alloys, which is shown in Fig. 6b. From the figure, it is evident that the hardness values increase rapidly with the copper addition from 0 to 0.75 wt.% (C0 to C3 alloy), then a further increase in copper alloying does not show much effect on the hardness. Rooney et al. [20] also found an improvement in tensile strength values in grey cast iron with copper addition and stated that the pearlitic transition was the major reason for the increase in tensile strength of cast iron. The impact strength of the grey cast

iron alloy decreases drastically from C0 to C1. There is an observable change that occurs in C2 and C3 alloys while C4 shows a mild drop in impact strength value. Impact strength decreases with a decrease in ferrite content but the copper addition mildly increases the soft graphite in the microstructure which may be the reason for the mild decrease in impact strength. Upadhyay and Saxena [21] reviewed that the decrease in impact strength in grey cast iron with copper addition is attributed to the microstructural transition from ferrite to pearlite phase with copper addition. The optimum copper addition for the production of the cylindrical blocks with matching tensile strength (262 MPa), hardness (202 BHN), and impact strength (3.5 Joule) is found at 0.48 wt.% Cu. The matrix is also composed of 99.68% pearlite and 99.38% of A-type graphite flakes at this composition.

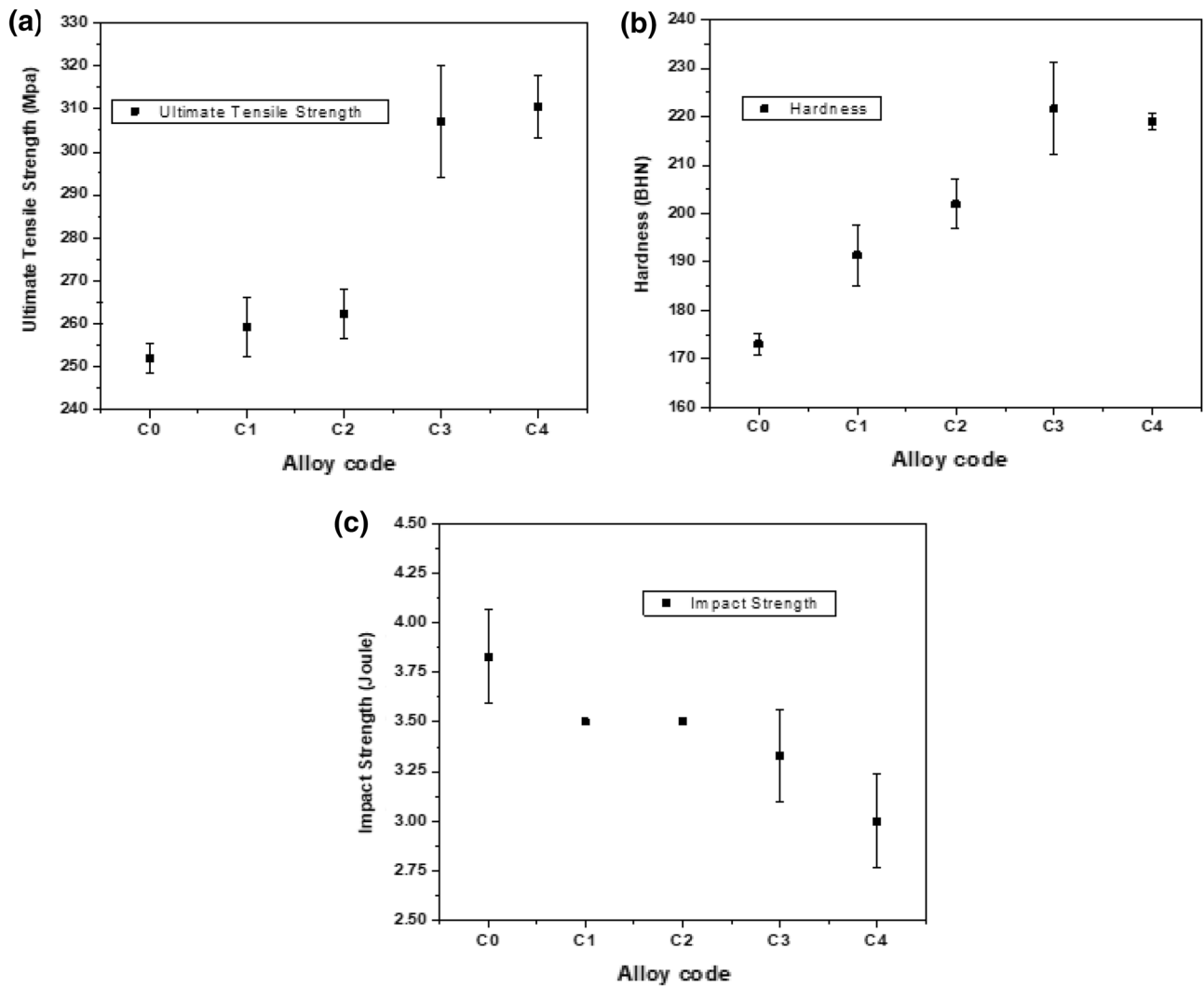


Fig. 5 Effect of copper alloying on mechanical properties of grey cast irons, **a** Ultimate tensile strength, **b** Hardness, **c** Impact strength

Table 5 Effect of Cu percentage variation in grey cast iron on ultimate tensile strength, hardness and impact strength

Sample no	Composition		UTS (MPa)		Hardness (BHN)		Impact strength (Joule)	
	%Cu Added	%Sn Added	Value	R ²	Value	R ²	Value	R ²
C0	0.00	0.00	252	3.56	173	2.16	3.83	0.23
C1	0.25	0.05	259.25	6.86	191.33	6.34	3.5	0.00
C2	0.50	0.05	262.33	5.79	202	5.10	3.5	0.00
C3	0.75	0.05	307.04	12.87	221.67	9.57	3.33	0.23
C4	1.0	0.05	310.47	7.39	219	1.63	3.0	0.23

3.4 Fractography

The grey cast iron is supported by graphite flakes and pearlite matrix (> 90%). During tensile deformation of grey cast iron, pull out or decohesion of graphite flakes is the mechanism that commences the fracture process as these are the

stress concentrators in the matrix. Later on, the entire load is supported by a pearlite matrix, which shows quasi-cleavage fracture surfaces upon deformation. The bright fracture surface (due to the presence of cementite) on the peripheries is indicative of brittle fracture and dimples in the inner region (due to the ferrite fracture) upon deformation suggests

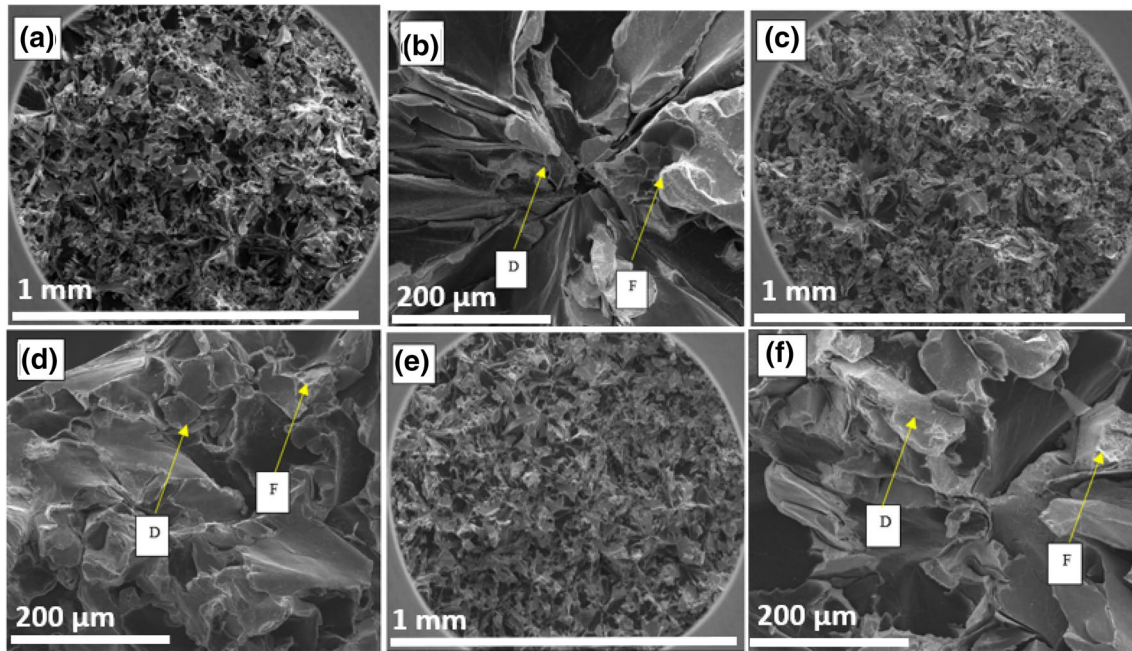


Fig. 6 SEM fractography study of the fractured surface of grey cast iron samples and grey cast iron alloyed with copper variation and tin kept constant during tensile testing **a & b** 0.25 wt.% Cu, **c & d**

0.5 wt.% Cu, **e & f** 1.0 wt.% Cu, ((Arrow D) shows the area of decohesion of flakes from the matrix and (Arrow F) shows a small area of the fracture)

ductile fracture. Figure 6a, b shows the fracture surfaces of the base metal revealing holes due to the graphite pull-out, bright outer fracture surface and inner dimples in the micrographs. The size of the holes and dimple fracture in the fracture surfaces decrease with increased copper alloying (0.5 wt.% Cu and 0.1 wt.% Cu), which are shown in Fig. 6c, d, e, f. The addition of copper stabilizes and refines the pearlite phase in presence of co-alloying elements because of its high austenitic stability [5]. Bermont and Castillo [22] also stated that in the pearlitic matrix grey cast iron the fracture mode during tensile loading could be explained by the holes formed due to graphite pull-out and quasi-cleavage type of mechanism.

4 Conclusions

The effect of copper content on the microstructural and mechanical properties of the grey cast iron alloys used in cylinder block applications has been studied. The tensile strength and hardness increase with an increase in copper content in the grey cast iron up to 0.72 wt.% and there is not much change observed as the copper content increases. Whereas, the impact strength decreases with the copper alloying. The increase in the tensile strength and hardness of alloys with copper content is due to the matrix change from ferrite to pearlite with copper alloying. The decrease in graphite flake aspect ratio is also the reason for the increase

in tensile strength and hardness with copper alloying. There is no observable variation in the chill depth with copper addition in grey cast iron. The optimum copper addition for the production of the cylindrical blocks with matching tensile strength (262 MPa), hardness (202 BHN), and impact strength (3.5 Joule) is found at 0.48 wt.% Cu. The matrix is also composed of 99.68% pearlite and 99.38% of A-type graphite flakes at this composition. Through the addition of cheap copper (compared to Mo and Ni) as an alloying element, the overall cost of the production also decreases.

Acknowledgements We are thankful to our Foundry Division management who has allowed us to do the study on optimization of alloying elements for making higher grade grey cast iron and thankful to the Tata Motors management for allowing us to publish a paper in the journal.

References

1. Oloyede O, Bigg T D, and Cochrane R F, *Mater. Sci. Eng. A* **654** (2016) 143. <https://doi.org/10.1016/J.MSEA.2015.12.020>
2. Yang W J, Pang J C, Wang L, Wang S G, Liu Y Z, Hui L, Li S X, and Zhang Z F, *Mater. Sci. Eng. A* **814** (2021) 141244. <https://doi.org/10.1016/J.MSEA.2021.141244>
3. König M, and Wessén M, *Int. J. Cast Met. Res.* **22** (2013) 164. <https://doi.org/10.1179/136404609X367597>
4. Tsujikawa M, Matsumoto N, Nakamoto K, and Michiura Y, *Key Eng. Mater.* **45** (2011) 151. <https://doi.org/10.4028/WWW.SCIEN.TIFIC.NET/KEM>

5. Labrecque C, and Gagne M, *Can. Metal. Q.* **37** (1998) 343. <https://doi.org/10.1179/cm.1998.37.5.343>
6. Lacaze J, and Sertucha J, *Int. J. Cast Met. Res.* **29** (2016) 74. <https://doi.org/10.1080/1364046120161142238>
7. Agunsoye J O, Bello S A, Hassan S B, Adeyemo R G, and Odii J M, *J. Min. Mater. Char. Eng.* **02** (2014) 470. <https://doi.org/10.4236/JMMCE.2014.25048>
8. Selin M, Holmgren D, and Svensson I L, *Mater. Sci. Forum* **649** (2010) 171. <https://doi.org/10.4028/WWW.SCIENTIFIC.NET/MSF.649.171>
9. Tsujikawa M, Nagamine K, Ikenaga A, and Hino M, *Int. J. Cast Met. Res.* **21** (2013) 76. <https://doi.org/10.1179/136404608X361701>
10. Kumar D T A, Kumar K G B, Pattanaik A, and Mukherjee M, *Trans. Indian Inst. Met.* **73** (2020) 3105. <https://doi.org/10.1007/S12666-020-02120-6/TABLES/4>
11. ASTM-A367 Standard Test Methods of Chill Testing of Cast Iron, Document Center, Inc. <https://www.document-center.com/standards/show/ASTM-A367>.
12. Rivera G, Calvillo P R, Boeri R, Houbaert Y, and Sikora J, *Mater. Charact.* **59** (2008) 1342. <https://doi.org/10.1016/J.MATCHAR.2007.11.009>
13. Bates C E, *Trans. AFS* **92** (1984) 923.
14. ELsawy E E T, El-Hebeary M R, and El Mahallawi I S E, *Wear* **390–391** (2017) 113. <https://doi.org/10.1016/J.WEAR.2017.07.007>
15. Sertucha J, Larranaga P, Lacaze J, and Insausti M, *Int. J. Met.* **4** (2015) 51. <https://doi.org/10.1007/BF03355486>
16. Siswanto A, Widodo R, and Ardiansyah E, *J. Phys. Conf. Ser.* **1450** (2020) 012127
17. Stefanescu D M, *Classification and Basic Metallurgy of Cast Iron. Properties and Selection: Irons, Steels, and High-Performance Alloys* (1990), p 3. <https://doi.org/10.31399/asm.hb.v01.a0009206>
18. König M, and Wessén M, *Int. J. Cast Met. Res.* **22** (2009) 164. <https://doi.org/10.1179/136404609X367597>
19. Poolthong N, Nomura H, and Nomura T, *Int. J. Cast Met. Res.* **15** (2016) 523. <https://doi.org/10.1080/13640461.2003.11819538>
20. Rooney T C, Wang C C, Rosenthal P C, Loper C, and Heine R, *Trans. AFS* **79** (1971) 189.
21. Upadhyay S, and Saxena K K, *Mater. Today Proc.* **26** (2020) 2462. <https://doi.org/10.1016/j.matpr.2020.02.524>
22. Bermont V M, and Castillo R N, *Int. J. Cast Met. Res.* **16** (2016) 257. <https://doi.org/10.1080/13640461200311819592>

Publisher's Note Springer Nature remains neutral with regard to jurisdictional claims in published maps and institutional affiliations.

Springer Nature or its licensor (e.g. a society or other partner) holds exclusive rights to this article under a publishing agreement with the author(s) or other rightsholder(s); author self-archiving of the accepted manuscript version of this article is solely governed by the terms of such publishing agreement and applicable law.